Chapter 2

Variability in Sun's magnetic field due to irregular properties of BMRs

"An equation means nothing to me unless it expresses a thought of God."

– Srinivasa Ramanujan

It is observed that the large-scale poloidal component of the magnetic field is produced due to the decay and dispersal of the tilted Bipolar Magnetic Regions (BMRs) on the solar surface. This poloidal field acts as the seed for the toroidal field and thus the next solar cycle. However, various properties of BMR, namely, the tilt, time delay between successive emergences, emergence latitude, and flux, all have irregular variations. These variations can lead to changes in the polar field and consequently variations in the solar cycle. In the present study, using the 3D kinematic dynamo model STABLE, we quantify the variation in the polar field and the solar cycle by considering randomness in different properties of BMR inspired by the observations. We find that randomness in the time delay between BMR emergence produces a negligible variation in the polar field and the solar cycle. However, the variation in BMR latitude and flux produce substantial effects,

while the scatter in the tilt around Joy's law produces the largest variation. Thus, this study suggests that in addition to the variation in the BMR tilt, the observed variations in BMR flux and latitudinal position are the two additional causes for the variabilities in the polar field and the solar cycle.

2.1 Introduction

The 11-year magnetic cycle in the Sun exhibits irregularities. The extreme variation in the cycle can be seen as grand minima such as the Maunder minimum and grand maxima namely the modern maximum (Biswas et al., 2023b). Besides the long-term modulation, the sun also exhibits short-term variations (6 – 18 months), known as bursts of activity or sun seasons (Gurgenashvili et al., 2016; Rieger et al., 1984) , as well as double peaks in the solar cycle (Karak et al., 2018). Waldmeier (1935) reported that the strong cycles take less time to rise and vice versa (also see Cameron & Schüssler, 2016; Karak & Choudhuri, 2011). Hence, the variation in the amplitude and duration of the cycle is somewhat related. Furthermore, the Sun's polar field shows irregular variations, and the timing of its polarity reversal is not consistent, differing from one cycle to another by several months to years (Golubeva et al., 2023). In fact, there are evidence of possible triple reversals of the polar field (Makarov et al., 1983; Mordvinov et al., 2022). Because of this variable nature of the solar cycle, it is challenging to make a prediction of the future solar cycle (Petrovay, 2020).

As we have discussed in the §1.4, the solar magnetic cycle is the result of a dynamo operating in the SCZ and thus the variability observed in the solar cycle must be connected to the dynamo action (Karak, 2023). There are enough evidence that the solar dynamo is of $\alpha\Omega$ type (Cameron & Schüssler, 2015; Charbonneau, 2020; Karak et al., 2014) in which the α denotes the generation of poloidal field from the toroidal one (the α effect) and the Ω represents the Ω effect in which the toroidal field is generated from the poloidal one through the differential rotation. Since the large-scale poloidal field generated

through Babcock–Leighton mechanism in the Sun §1.4. Hence, we shall consider this Babcock–Leighton process for the generation of the poloidal field in our solar dynamo model.

In the solar dynamo model, the Babcock–Leighton process is a crucial component which involves randomness. The extensive randomness arises in the Babcock–Leighton process through the tilt angle of BMR. Observations also show that there is a considerable amount of scatter in tilt angle around the Joy's law (Howard, 1991; Jha et al., 2020; Sreedevi et al., 2023). While in most of the previous studies, the tilt is measured from the sunspot group (when magnetograms data are not available; Sivaraman et al., 2007) or BMR by repeatedly observing the same feature (e.g., McClintock & Norton, 2016), recently Sreedevi et al. (2023) have tracked the BMRs for the last two solar cycles and produced unique tilt for each BMR during this period. Figure 4 of Karak (2023) shows Joy's law and the scatter around the tilt obtained from those tracked BMRs. The scatter around the tilt is found to be a primary cause of fluctuations in the Babcock–Leighton process (Jiang et al., 2014; Karak & Miesch, 2017). Furthermore, observations show that about 8% of BMRs in a solar cycle are anti-Hale (McClintock et al., 2014) while 25 to 30% are non-Joy. These anti-Hale BMRs produce opposite polarity field and thus they disturb the regular polar field (Cameron et al., 2013; Jiang et al., 2014; Karak & Miesch, 2018; Karak et al., 2018; Kitchatinov et al., 2018; Mordvinov et al., 2022; Pal et al., 2023). Nagy et al. (2017) showed that in the extreme case, a sufficiently complex wrongly tilted (rogue) BMRs can disturb the dynamo and it may lead to a grand minima.

The other sources of irregularity in the solar dynamo are the time delay in the BMR emergence, latitude position, and the flux of BMR. It has been observed that the time delay between two successive BMRs is not the same, and it follows a distribution. Again from the tracked BMRs from MDI and HMI for the last two solar cycles (Sreedevi et al., 2023), as presented in Figure 2.1(a), we find that the lag between two successive BMR

emergences follow a distribution which can be approximated by a log-normal distribution. This distribution in the time delay of BMR emergence can introduce a variation in the solar cycle. A related time delay in the solar dynamo is the delay in the rise of the BMR-forming toroidal flux tube from the base of the CZ to the surface; see Sects. 5.3 and 6.4 of Karak (2023). When this delay is magnetic field dependent, it can lead to a variation in the solar cycle (Jouve et al., 2010b). The latitude of BMR emergence on the solar surface is also not uniform. The mean latitudes of BMRs in a cycle depends on its strength (Jiang et al., 2014; Mandal et al., 2017; Solanki et al., 2008; Waldmeier, 1955). As a result, in the strong cycles, BMRs begin at high latitudes. Jiang (2020); Karak (2020); Petrovay (2020) showed that systematic variation in the latitudes of emerging BMRs has a nonlinear effect which can act as the amplitude-limiting mechanism in the Babcock–Leighton type dynamos. Finally, the flux content in the erupting BMR is not constant, and it randomly varies roughly in the range of 10^{21} to 10^{23} Mx following a log-normal distribution as seen in Figure 2.1(b); also see Sheeley (1966). Variation in the BMR flux can cause a change in the poloidal field and thus the sunspot cycle.

Since the polar magnetic field or its proxy is strongly correlated with the activity level of the next cycle (Choudhuri et al., 2007; Kitchatinov & Olemskoy, 2011; Kumar et al., 2021a, 2022; Muñoz-Jaramillo et al., 2013; Priyal et al., 2014; Schatten et al., 1978; Wang & Sheeley, 2009), the variation of the polar field can cause a variation in the solar magnetic cycle. Therefore, to realize the behavior of the future solar cycle, it is essential to understand the polar field of the present cycle. In this chapter, we have quantified the variation of the polar field generated in a cycle, caused by the variations in (i) the time delay of successive BMR eruptions, (ii) the BMR flux, (iii) the BMR tilt angle, and (iv) the latitude of BMR eruption. We shall perform simulations using synthetic BMR data deposited in our 3D kinematic dynamo model STABLE (Surface Flux Transport and Babcock–Leighton) and analyze the polar field and solar cycle variation.

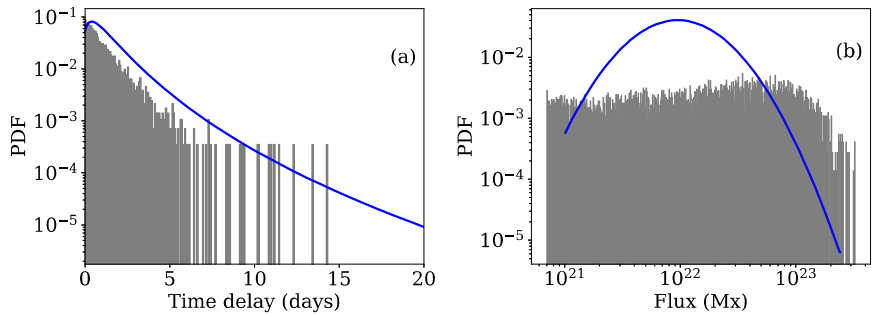

Fig. 2.1 Distributions of (a) the time delay between two successive BMR emergences and (b) flux content of 8800 BMRs obtained from MDI and HMI magnetograms during 1996–2020. Quantities are obtained by tracking each BMR throughout its lifetime or disk passage and taking the average values during the time when the flux is above 70% of its maximum (Sreedevi et al., 2023). The solid lines are the log-normal distributions that approximately fit the data and they will be used in our calculations and was also used in Karak & Miesch (2017).

2.2 Model

In this work, we have used a 3D kinematic dynamo model STABLE (Karak & Miesch, 2017; Miesch & Dikpati, 2014; Miesch & Teweldebirhan, 2016). BMRs in this model are deposited based on the toroidal magnetic field present at the base of CZ, and the decay and dispersal of BMRs near the surface produce the poloidal field. The poloidal field eventually gives rise to the toroidal one through differential rotation and sustains the dynamo loop. This model can also be operated as a surface flux transport (SFT) model if we deposit BMRs on the solar surface. Karak & Miesch (2018) showed that this model also produces the correct latitude-dependent variation of the polar field—higher the latitude of BMR emergence, lower is the polar field generated. Karak (2020) showed that this effect leads to so-called latitude quenching which was suggested by Jiang (2020); Petrovay (2020) based on the SFT model and observation.

To demonstrate the performance of the STABLE model as SFT explicitly, we present the axial dipole moment (DM) produced from a BMR deposited at different latitudes in

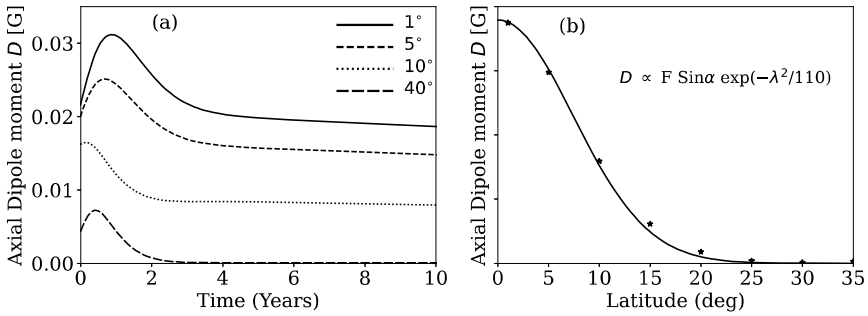

Fig. 2.2 The results produced from STABLE dynamo model. (a) Time evolution of the axial dipole moment (D) of a BMR deposited at different latitudes with constant flux (F) of 10^{22} Mx and tilt (α) of 80°. (b) The values of the saturated (final) dipole moment vs the latitude of single BMR. The solid curve is the Gaussian fit of the form $\exp(-\lambda^2/110)$.

Figure 2.2. We observe that the STABLE model also captures the behavior as seen in the SFT model, namely with increasing the latitude of the BMR emergence the generation of DM decreases (Figure 2.2(a)) and the final saturated dipole moment produced can be approximated by a Gaussian profile as predicted by the SFT models (Jiang et al., 2014; Petrovay et al., 2020). We would like to mention that Hazra et al. (2017) failed to capture this feature as they did not include a downward pumping which is essential to make the model consistent with observations and SFT models (Cameron et al., 2012; Karak & Cameron, 2016).

In the present study, we shall exploit this feature of the STABLE dynamo model and utilize it as a dynamo simulator to study the solar cycle variation and as an SFT model to study the polar field evolution. The advantage of using STABLE as an SFT model is that we can have better control of BMR properties (tilt, flux, separation of BMR, spatial distribution, and emergence rate of the BMRs), and we can treat it as a testbed to explore the effect of various properties of BMR on the polar field. In the next subsection, we first describe the STABLE model.

2.2.1 STABLE model

In this model, we solve the Induction equation in three dimensions (r, θ, ϕ) for the whole CZ with $0.69R \leq r \leq R$ (R is the radius of the sun), $0 \leq \theta \leq \pi$, and $0 \leq \phi \leq 2\pi$.

$$\frac{\partial \boldsymbol{B}}{\partial t} = \nabla \times \left[(\boldsymbol{V} + \boldsymbol{\gamma}) \times \boldsymbol{B} - \eta_t \nabla \times \boldsymbol{B} \right], \tag{2.1}$$

where $\boldsymbol{V}$ is the velocity field such that

$$\boldsymbol{V} = v_r(r,\theta)\hat{r} + v_\theta(r,\theta)\hat{\theta} + r\sin\theta\Omega(r,\theta)\hat{\phi}. \tag{2.2}$$

Here the axisymmetric velocity field is composed of meridional circulation v_r, v_θ, and the differential rotation ($\Omega = v_\phi / r\sin\theta$). The profile of Ω used in this model roughly captures the observed properties as inferred through helioseismology (Schou et al., 1998) and was used in Karak & Miesch (2017). For the meridional circulation, we have considered a single cell circulation profile as used in Karak & Cameron (2016). In Equation (2.1), $\boldsymbol{\gamma}$ represents the magnetic pumping which helps to suppress the loss of the toroidal field through the surface and thus boosts the dynamo efficiency even at high diffusivity (Karak & Cameron, 2016). Our model includes a radially downward magnetic pumping of speed 20 m s^{-1} in the near-surface layer ($r \geq 0.9R$) of the sun. In this model, we have considered a radial-dependent effective turbulent diffusivity η_t of order 10^{12}cm^2 s^{-1} (4.5×10^{12}cm^2 s^{-1}for $r \geq 0.956R$ and 1.5×10^{12}cm^2 s^{-1} below) throughout the whole CZ. Below the CZ the magnitude of the diffusivity is reduced by about four orders of magnitude.

A crucial part of this model is the Spotmaker algorithm, which places a BMR on the surface when certain conditions are satisfied. The first condition for generating a BMR is that the magnetic field strength at the base of CZ must exceed a critical field strength B_c. We have made B_c latitude dependent such that it makes BMR emergence difficult at high latitudes and it helps the model BMRs to be consistent with the observations (Karak,

2020). The second condition is the time delay between successive BMR emergence. After the first BMR eruption, the time delays for the subsequent eruptions are taken from the observed log-normal distribution as shown in Figure 2.1(a), which follows the profile:

$$P(\Delta) = \frac{1}{\sigma_d \Delta \sqrt{2\pi}} \exp\left[\frac{-(\ln \Delta - \mu_{\rm d})^2}{2\sigma_d^2}\right], \tag{2.3}$$

where σ_d and μ_d are specified as, $\sigma_d^2 = \frac{2}{3}\left[\ln \tau_s - \ln \tau_p\right]$ and $\mu_d = \sigma_d^2 + \ln \tau_p$. Here $\tau_p = 0.8$ and $\tau_s = 1.9$ and Δ is the time delay between two successive BMRs (normalized to one day).

Now we have to specify the properties of BMRs (tilt, flux, and separation) in this model. We take a log-normal distribution of flux that is close to the observed one, as shown in Figure 2.1(b).

$$P(\phi) = \phi_0 \frac{1}{\sigma_\phi \phi \sqrt{2\pi}} \exp\left[\frac{-(\ln \phi - \mu_\phi)^2}{2\sigma_\phi^2}\right], \tag{2.4}$$

where $\mu_\phi = 51.2$ and $\sigma_\phi = 0.77$. We have specified the BMR field strength at the surface as 3 kG. For the separation of BMRs, we choose the half distance between the centers of two spots of BMR to be 1.5 times the radius of the spot. For the tilt angle of BMRs, we follow the standard Joy's law: $\delta = \delta_0 \cos\theta$ (Dasi-Espuig et al., 2010; Stenflo & Kosovichev, 2012), where θ is co-latitude and $\delta_0 = 35^\circ$. The fluctuations included in the tilt follow a Gaussian distribution with $\sigma_\delta \approx 15^\circ$ (Jha et al., 2020; Karak, 2023; Wang et al., 2015).

Further, we discuss the nonlinearity needed to limit the growth of the magnetic field. In our model, the latitude-dependent BMR threshold introduces a nonlinearity, so-called latitude quenching (Jiang, 2020; Karak, 2020). This helps to stabilize the growth of the magnetic field in our model. In addition to this, we include a magnetic field-dependent quenching of the form: $1/\left[1 + (B/B_0)^2\right]$ in the tilt of BMR (tilt-quenching), inspired by the observations (Jha et al., 2020).

2.2.2 Deposition of synthetic BMRs in STABLE

Now we discuss how instead of using the SpotMaker algorithm, we can feed synthetic BMR data into STABLE to operate this as SFT model. Following Jiang et al. (2018), we develop a synthetic BMR generation code to produce smoothed monthly synthetic BMR data. The following equation can describe this.

$$\overline{F}_{sm}(t) = f_2(t) + \overline{\Delta r(t)} f_2(t). \tag{2.5}$$

Here

$$f_2(t) = \frac{at^3}{\exp\left[\frac{t^2}{b^2}\right] - c}, \tag{2.6}$$

where t is time in month, $a = \left(\frac{S_n}{9072.8}\right)^{\frac{1}{0.706}}$ with S_n the amplitude of the sunspot cycle, $b = 27.12 + \left(\frac{25.15}{1000a}\right)^{\frac{1}{4}}$, and $c = 0.71$.

When $t < 72$ months,

$$\overline{\Delta r(t)} = 8.68 \exp\left(\frac{-z_1^2}{2}\right), \tag{2.7}$$

with $z_1 = \frac{t-200.44}{45.86}$.

When $72 \leq t \leq 108$ months, then

$$\overline{\Delta r(t)} = 2.64 \exp\left(\frac{-z_2^2}{2}\right), \tag{2.8}$$

with $z_2 = \frac{t-149.0}{27.31}$.

Finally in the last phase, when $t > 108$ months, the synthetic BMR follows the given profile:

$$\overline{F}_{sm}(t) = f_2(t). \tag{2.9}$$

After getting synthetic BMRs, we need to specify the properties of these BMRs. The mean latitude of the BMRs distribution λ_n depends on the cycle strength S_n and it follows

the profile:

$$\lambda_n(t) = \left[26.4 - 34.2\frac{t}{T_{cy}} + 16.1\left(\frac{t}{T_{cy}}\right)^2\right]\frac{\overline{\lambda}_n}{14.6}, \tag{2.10}$$

where $\overline{\lambda}_n = 12.2 + 0.015S_n$ and T_{cy} is the cycle period in month. The scatter in latitude distribution obeys a Gaussian profile with σ defined as:

$$\sigma = \left[0.14 + 1.05\frac{t}{T_{cy}} - 0.78\left(\frac{t}{T_{cy}}\right)^2\right]\lambda_n(t). \tag{2.11}$$

We consider synthetic BMR emergence symmetric in both hemispheres, and the longitudinal distribution of BMRs are random. The BMR eruption time delay is taken randomly within a month, and the flux distribution is decided by Equation (2.4). The tilt is taken from the same prescription as discussed above for STABLE (Joy's law with Gaussian scatter). After giving a scatter of $\sigma_\delta \approx 15^\circ$, we have found 30 – 35% BMRs are anti-Hale and non-Joy. We have ensured that 25 – 30% of total BMRs would be non-Joy and about 8% would be anti-Hale as observational results suggest.

2.3 Results and Discussion

We first quantify the effect of randomness in BMR properties on the polar field using the STABLE dynamo model as SFT. Later we shall measure the variability of the solar cycle using the STABLE as a dynamo model.

2.3.1 Variation in the polar field

We feed synthetic BMR data for one cycle (of about 11 years long) in STABLE and perform simulations by operating it as SFT model with random variation in different BMR properties. For the statistical reliability of the result, we have repeated each case for 30 different realizations of the random number. As a reference case, we first perform

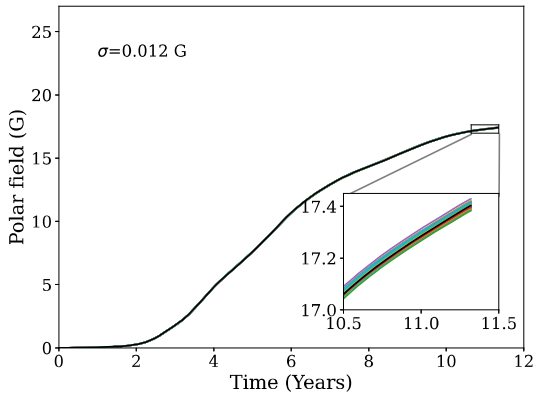

Fig. 2.3 The plot shows the effect of time delays in successive BMR eruptions on the polar field. The black curve shows a reference polar field in the plot (see inset for the zoomed-in view).

Table 2.1 Variability σ and the maximum possible percentage variability produced in the polar field due to different individual fluctuation parameters of the BMRs relative to the combined fluctuations (Figure 2.4(d); $\sigma = 2.39$ G).

Variable Parameters	Variability (σ) G	Max. % variability
Time delay	0.012	0.5%
Latitude	0.330	13.8%
Flux	1.156	48.3%
Tilt scatter	1.624	68.7%

a simulation without adding any random component in the BMR properties. For the quantification of the polar field, we compute the remnant magnetic flux strength from 55° latitude to the pole in the northern hemisphere. The variation of this polar field for the reference case is shown by the black curve in all the Figure 2.3 – 2.4.

Due to the irregular time delay of BMR eruption

The time evolutions of the polar fields obtained from the simulations with the different realizations of the time delay are shown by different colors in Figure 2.3. We find that these curves deviate only negligibly from the reference polar field (see black curve and the inset) and the standard deviation from the reference polar field is $\sigma = 0.012$ G; see

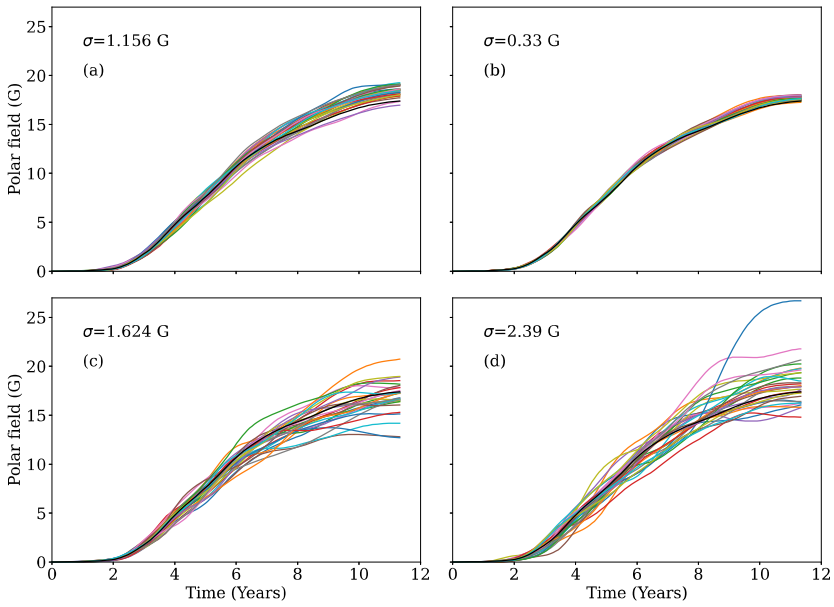

Fig. 2.4 Format of each panel is the same as Figure 2.3, but shows the evolution of the polar field from simulations with (a) variation in the BMRs flux, (b) variation in BMRs latitude, (c) scatter in BMR tilt, and (d) combined fluctuations.

Table 5.1. The reason for the tiny changes in the polar field is the following. The most probable time delay of the BMR emergence rate is less than a day (mode of the distribution is 0.8 days and mean is 1.9 days; see Figure 2.1(a) and the probability decreases with increasing the time delay. When the time delay is 10 days, the probability of the BMR emergence is less than 1%. In contrast, the polar field takes about 1 to 2 years to reach the pole from the active latitude belt where it is formed. Hence, the variation in the polar field caused by the variation in the time delay is smoothed out by the time it reaches the pole, and we observe only a negligible variation. We note that when we performed different simulations at different realizations of random delay, we kept the total number of BMRs in one month the same. Instead of this, if we increase this time to six months, then we also find a tiny variation in the polar field with respect to the reference case. Hence, based on

these simulations, we conclude that the randomness in the time delay introduces only a slight variation in the polar field.

Due to variation in BMR flux

Now we analyze the result of the simulations with variation in the BMR flux, keeping all other parameters of the BMR invariant. Figure 2.4 (a) shows the variation of the polar field for this case. Now we observe a noticeable variation in the evolution of the polar field. The standard deviation from the reference polar field is found to be $\sigma = 1.156$ G. A variation, in this case, is expected because the contribution to the polar field in a given hemisphere from decayed active region flux would be proportional to the total hemispheric active region flux (Kitchatinov & Olemskoy, 2011; Petrie, 2015). Therefore, the variation in the BMR flux is one cause of variation in the polar field.

Due to variation in the BMR latitude

Variation in the latitude distribution of BMR also gives a variation in the polar field strength ($\sigma = 0.33$ G) . This is shown in Figure 2.4 (b) in which we present the time evolution of the polar field from simulations at different realizations of the BMR latitudes. A variation in the polar field due to a change in the BMR latitude is expected because when BMRs appear at low latitudes, the cross-equatorial cancellation is much more effective than the BMRs which appear at higher latitudes, which has been demonstrated in Figure 2.2. Jiang et al. (2014); Karak & Miesch (2018) already showed that the latitudinal variation of BMRs affects the polar field strength (also see Mordvinov et al., 2022). We note that in our case, the variation in the polar field is less because the mean and the width of the latitude distribution remain the same in all the simulations while in the observed solar cycle, these vary with the cycle strength. Thus, our study shows that even when we keep the mean

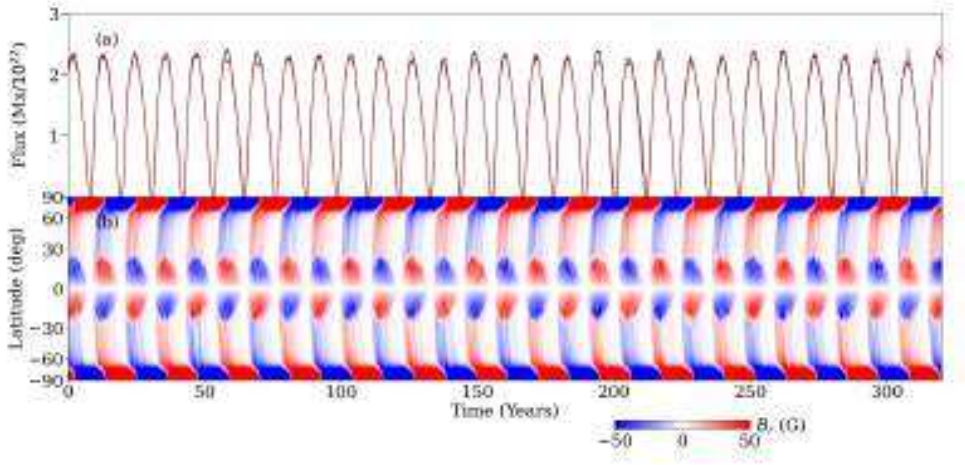

Fig. 2.5 Temporal variations of (a) the monthly numbers of BMRs (red/black: north/south) and (b) the azimuthal-averaged surface radial field from the simulations in which the time delay in BMR eruption is random.

latitudinal distribution of the BMR the same and vary the individual latitude of the BMR, we find a noticeable variation in the polar field.

Due to scatter in BMR tilt around Joy's law

Figure 2.4 (c) shows the effect of tilt scatter on the polar field variation ($\sigma = 1.624$ G). As in the Babcock–Leighton process, it is the tilt which makes the generation of the poloidal field possible in the Sun, any change in the tilt can certainly produce variation in the poloidal field. Particularly when we have a wrongly tilted BMR (non-Joy and anti-Hale), it produces an opposite polarity field (e.g., Mordvinov et al., 2022; Nagy et al., 2017). Recently, Pal et al. (2023) also showed that the emergence timing, relative numbers, latitude distribution, and flux content of anomalous active regions significantly impact the reversal timings and strength of the dipole moment. In our model, we have included about 30 to 35% non-Hale and non-Joy BMRs (consistent with observations). These anti-Hale and non-Joy BMRs having opposite tilts than regular BMRs generate the opposite polarity

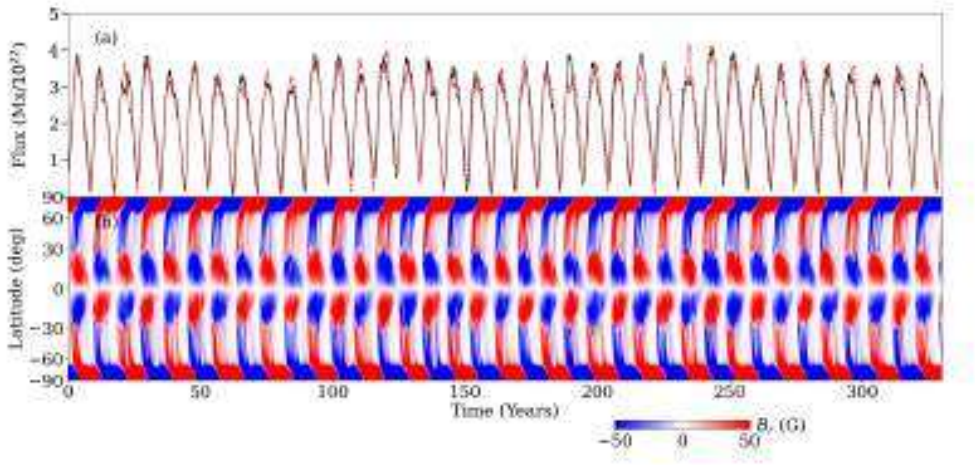

Fig. 2.6 Same as Figure 2.5 but from the simulation in which BMR flux is irregular.

field. This opposite polarity field brings about a large fluctuation in the polar field of our simulation. Previously Upton et al. (2021) also found that increasing the tilt scatter around Joy's law significantly increases the change in the polar axial dipole from one cycle to the next. By comparing the simulations presented in the previous three sections with randomness in BMR time delay, flux, latitude, and tilt, we conclude that the tilt scatter produces maximum variation in the polar field. For comparative variability in the polar field due to these parameters see Table 2.1.

Due to combined fluctuations

Now we measure the polar field variation due to the combined effect of all the fluctuations, i.e., the variations in tilt, time delay, flux, and latitude. This replicates the realistic scenario. Figure 2.4 (d) shows the polar field variation in this case. We find that in this case, the variation in the net polar field strength is highest ($\sigma = 2.39$). Maximum variation is expected because all individual random effects can contribute additively.

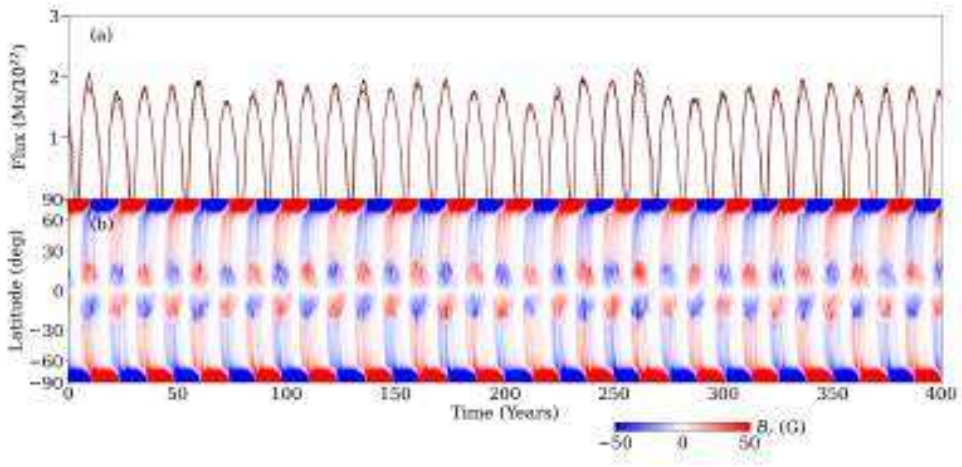

Fig. 2.7 Same as Figure 2.5 but from the simulation in which the tilt has a scatter around Joy's law.

2.3.2 Variation in the solar cycle

Now we study the variability of the solar cycle due to irregular properties of BMR by operating STABLE in default mode, i.e., as a dynamo model. For this, we consider three cases: (i) irregular time delay in the BMR eruption, (ii) irregular BMR flux, and (iii) scatter in BMR tilt angle around Joy's law. We note that to study solar cycle variation, we are not considering the case of the variation in the BMR latitude separately because it is not trivial to vary BMR latitude randomly by hand. When the cycle strength varies, the mean latitude of BMR varies hence it will be captured when cycle strength will vary. In STABLE, at every numerical timestep, a BMR latitude is chosen randomly out of the latitude points where the azimuthal field exceeds the threshold which is latitude dependent. Moreover, we have seen in §2.3.1 (Figure 2.4(b)) that in this case the variation in the polar field is less compared to the variations in the tilt and flux and thus we are not presenting any separate case with variation in the BMR latitude.

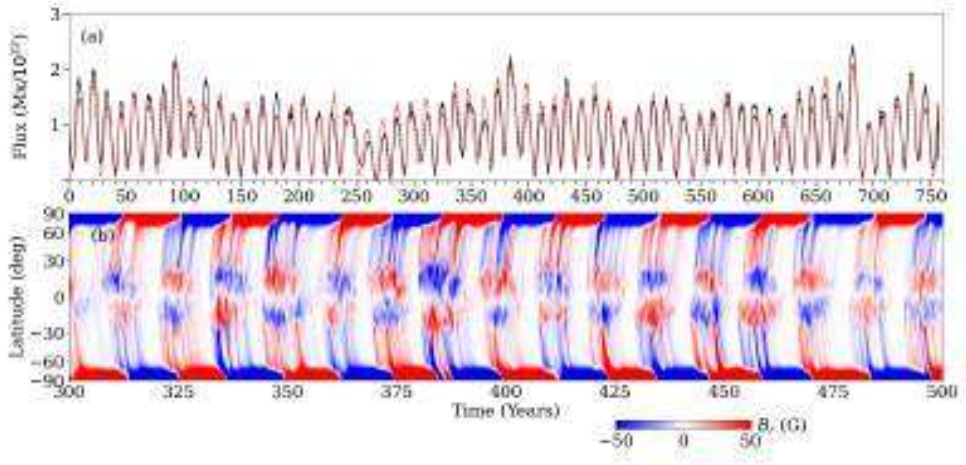

Fig. 2.8 Same as Figure 2.5 but from simulations including all fluctuations (i.e., time delay, flux, latitude, and tilt) and the time delays are magnetic field independent.

Figure 2.5 shows the solar cycle variability as measured by the monthly value of the BMR flux and the surface radial field as the function of time for the case in which the randomness in the BMR time delay is introduced. We find that the variability in the solar cycle in both hemispheres is negligible. In the polar field evolution §2.3.1, we have already seen that the random time delay in BMR eruption causes a negligible variation in the polar field. In the context of Babcock–Leighton dynamo, the poloidal field gives toroidal field which eventually produces BMRs on the solar surface. Therefore, a tiny variation in the polar field is expected to cause a tiny variation in the next solar cycle. While this expectation is based on the dynamo mechanism (e.g., Charbonneau & Barlet, 2011; Kumar et al., 2021a) and the observations (Muñoz-Jaramillo et al., 2013), if the dynamo operates in the chaotic region (much above the critical transition), even a small change in the polar field can lead to a large change in the solar cycle. However, it is important to note that our model does not operate within that specific region, and thus, such effects are not accounted for in our model. In summary, the simulation performed in this case indicates that irregular rate of BMR emergence does not produce significant variation in the solar cycle.

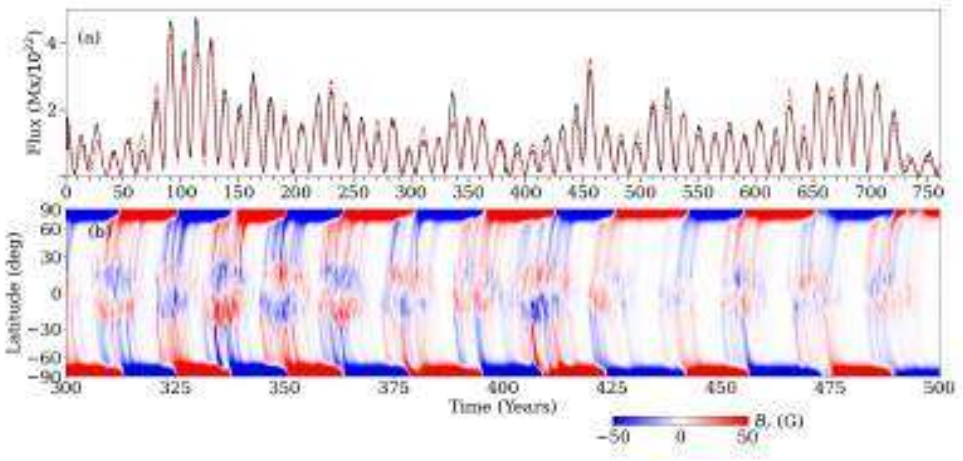

Fig. 2.9 Same as Figure 2.8 but with magnetic field-dependent time delay.

However, when we perform the dynamo simulation with the variation in BMR flux, we observe a considerable amount of long-term modulation in the solar cycle as seen in Figure 2.6. A considerable variation in the solar cycle is expected given the fact that it produces a significant variation already in the polar field as seen in §2.3.1. Next, when we consider the scatter in BMR tilt around Joy's law, we again find a considerable amount of variation in the solar cycle as seen in Figure 2.7. Again this result is congruous with the expectation that a considerable variation in the polar field is observed with the tilt scatter. Previous studies have also shown that the scatter in BMR tilt can produce large variations in the solar cycle, including grand minima and grand maxima (Karak & Miesch, 2017, 2018; Lemerle & Charbonneau, 2017; Nagy et al., 2017).

Now we perform two other simulations by including all the fluctuations mentioned above individually i.e., variation in time delay, flux, and tilt. The basic difference between these two simulations is the only time delay. In one simulation, the time delay is magnetic field independent (Figure 2.8) while in another it is magnetic field dependent (Figure 2.9). To make the time delay magnetic field dependent, we make the following changes in the

time delay parameters for both hemispheres:

$$\tau_p = \frac{2.2}{1+\left[\frac{B_b}{400}\right]^2}, \quad \text{and} \quad \tau_s = \frac{20}{1+\left[\frac{B_b}{400}\right]^2}, \tag{2.12}$$

where B_b is the azimuthal-averaged toroidal magnetic field in a thin layer spanning from $r = 0.715R$ to $0.73R$ at approximately 15° latitude.

We find more variability and grand minima-like appearance when the time delay is magnetic field dependent. However, in the magnetic field independent case, we observe a few triple reversals of the polar field; see reversal in the southern hemisphere between 375 – 400 years in Figure 2.8(b). We find triple reversal events in the magnetic field-independent time delay case because in this case, the emergence rate of BMRs does not change much over the solar cycle, while in the magnetic field-dependent case, it varies largely with the solar cycle—becoming highest around the solar maxima and lowest around the solar minima (because in this case the time delay is magnetic field dependent and varies according to the magnetic field strength). Therefore, in the magnetic field-independent case, the emergence rate around the cycle maxima is less (compared to the magnetic field-dependent case), and as the BMR number is less, the effect of tilt scatter (the non-Joy and anti-Hale BMR) is statistically more prominent. However, in the magnetic field-dependent case, the effect of tilt scatter largely cancels out due to the relatively large number of BMR emergences at the times of cycle maxima and this does not lead to triple reversals. Moreover, observations and models (Mordvinov et al., 2022) both reveal that the occurrence probability of triple reversal events is maximum around the time of solar cycle maxima.

Further, magnetic field-dependent and independent time delays produce variability in the solar cycle in a different way. Since grand minima and maxima-like events are more probable in the magnetic field-dependent time delay case, and the morphology of

the magnetic field better resembles the solar observation in this case, the magnetic field-dependent time delay case is more favorable with observation. Indeed, the distribution of the time delay in the observation varies with the solar cycle—becoming narrower during solar maximum, and thus it is magnetic-field dependent.

2.4 Conclusions

We have utilized the 3D STABLE dynamo model to identify the causes of the variations of the polar field and the solar cycle due to the stochastic properties of BMRs in the poloidal field generation (Babcock–Leighton process). Guided by the observations, we have considered the variations in the following processes: (i) time delay in BMR emergence, (ii) BMR flux, (iii) BMR latitude, and (iv) BMR tilt angle. We observe the least variability in the polar field and solar cycle due to the time delay in the BMR emergence. The maximum variability appears due to scatter in the BMR tilt. The flux content and latitude variation of BMR also produce significant variability in the polar field and the solar cycle. The combined effect of all these parameters on the variability of the solar cycle is the highest and they are sufficient to reproduce a large spectrum of the observed modulation in the solar cycle and magnetic field, including producing grand minima and maxima, and triple reversals of polar field. Our study suggests that in addition to the usual notion for the tilt angle to be the cause of solar cycle variability, the variations in the flux and latitudinal position of the BMR are also the two potential sources for the variability in the solar cycle.